ChemPubSoc Europe

DOI: 10.1002/cplu.201700047

CHEMPLUSCHEM Full Papers

Efficient Benzodithiophene/Benzothiadiazole-Based n-Channel Charge Transporters

Rafael Sandoval-Torrientes[+],[a] Joaquín Calbo[+],[b] Wakana Matsuda,[c] Wookjin Choi,[c] José Santos,[a] Shu Seki,*[c] Enrique Ortí,*[b] and Nazario Martín*[a, d]

A series of donor–acceptor small molecules based on electron-deficient benzothiadiazole (BTD) and electron-rich benzodithiophene (BDT) featuring an A-D-A structure is presented. Exhaustive spectroscopic, electrochemical, and computational studies evidence their electroactive nature and their ability to form well-ordered thin films with broad visible absorptions and low band gaps (ca. 2 eV). Time-resolved microwave conductivity (TRMC) studies unveil unexpected n-type charge transport displaying high electron mobilities around 0.1 $cm^2 V^{-1} s^{-1}$. Efficient electron transport properties are consistent with the low electron reorganization energies (0.11–0.17 eV) theoretically predicted.

Long-dreamed-of, light-weight, low-cost, and flexible electronic devices are close to becoming a reality. Advances in organic electronics have made it possible to improve not just the fabrication of the devices but also the properties of the active organic materials. Easy-to-process soluble organic semiconductors (OSC) with enhanced stability and electronic properties already are a reality.[1–3] Obtaining materials with high charge carrier mobilities (μ) is of the utmost importance, allowing faster operating transistors that save energy by reducing the calculation time, and also leading to more efficient organic photovoltaic (OPV) cells by improving the short-circuit current (J_{SC}). From a molecular point of view, it is the π-electronic coupling between the molecule's inner components, along with its lattice interactions with the neighboring molecules, that dictates the charge carrier transport properties and band gap. It has recently been demonstrated that incorporation of electron-deficient groups has a stabilizing effect since they reduce the electron density of the molecules (lowering in term■turn? ■ the HOMO energy).[4] In this sense, the combination of electron-rich π-conjugated polyaromatic heterocycles (overwhelmingly thiophene derivatives) as donors (D) with electron-deficient moieties as acceptors (A) in A-D-A motifs has emerged as an efficient strategy to improve both stability and intermolecular packing.

Compounds bearing benzothiadiazole (BTD) fragments are found widespread in fields ranging from drug design[5–7] to organic electronics. BTD has been extensively applied in the latter due its remarkable electron-accepting properties. Besides, its ability to lower the band gap by generating ground-state quinoid structures when flanked by five-membered aromatic rings, has allowed the synthesis of a number of materials with excellent photovoltaic response.[8–11] However, despite their widespread use in OPV devices, most of the reported systems are related with ■mentioned in terms of ■ their incorporation into polymeric materials and there are few studies of BTD-based small-molecule systems being applied as charge transporters.[12–14] The lack of studies, and the relevance the BTD fragment has recently gained, prompted us to investigate this electron-deficient group in a series of molecules featuring A-D-A architectures. The benzodithiophene (BDT) donor fragment is ubiquitous in most of the moderate-to-high-efficiency small-molecule OPV devices and some polymeric organic field-effect transistors (OFETs). Its association with BTD in A-D-A structures has showed potential for application in high-performance organic solar cells,[15]although their application in OFETs has not been yet tested. All previously reported systems bearing BTD units display (apparently without any reason) the same substitution pattern at the 4- and 7-positions. In this work we have decided to investigate the effect of the substitution at position 5 of the BTD in an A-D-A configuration as shown in Scheme 1. Interestingly, in addition to the easy ■ready■ synthetic availability of these compounds, they exhibited a less-explored n-type semiconducting behavior.

[a] R. Sandoval-Torrientes,[+] Dr. J. Santos, Prof. N. Martín
Instituto Madrileño de Estudios Avanzados (IMDEA)–Nanociencia
c/ Faraday, 9, 28049 Madrid (Spain)
E-mail: nazmar@ucm.es

[b] J. Calbo,[+] Prof. E. Ortí
Instituto de Ciencia Molecular
Universidad de Valencia
46980 Paterna (Spain)
E-mail: enrique.orti@uv.es

[c] W. Matsuda, W. Choi, Prof. Dr. S. Seki
Department of Molecular Engineering, Kyoto University
Nishikyo-ku
Kyoto 615-8510 (Japan)
E-mail: seki@moleng.kyoto-u.ac.jp

[d] Prof. N. Martín
Departamento de Química Orgánica
Facultad de C. Químicas
Universidad Complutense de Madrid
28040 Madrid (Spain)

[+] These authors contributed equally.

Supporting information and the ORCID identification number(s) for the author(s) of this article can be found under http://dx.doi.org/10.1002/cplu.201700047.

This article is part of a Special Issue on "Novel Aromatics". A link to the issue will appear here once it is compiled.

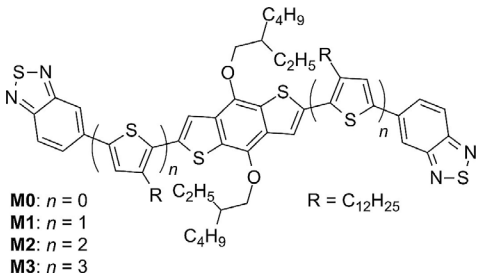

Scheme 1. BTD–BDT–BTD systems with thiophene bridges of increasing length.

As shown in Scheme S1 in the Supporting Information (SI), the benzothiadiazole component was obtained by reaction of 4-bromo-1,2-diaminobenzene with thionyl chloride following a previously reported method.[16] The resulting brominated product was coupled with a benzodithiophene organotin derivative by a Stille cross-coupling reaction to yield product **M0**. This orange-red solid showed a noticeably upfield shift (at $\delta =$ 7.84 ppm) for the singlet belonging to the BDT aromatic protons, allegedly attributed to■which is rationalized by■ the strong electron-withdrawing effect of the BTD unit. The BTD component could be modified by attaching a thiophene unit to the brominated benzothiadiazole through a cross-coupling reaction with tributyl(4-dodecylthiophen-2-yl)stannane, yielding a pale yellow solid. This product was brominated with *N*-bromosuccinimide (NBS) and then coupled to a thiophene organotin derivative. These last two steps could be repeated to provide BDT units bearing thiophene bridges of increasing length (see Scheme S1). These final product precursors exhibit the characteristic d, d, dd patterns in the ^{1}H NMR spectra of 4-substituted BTDs (signals at $\delta \approx$8.15, 8.00, 7.90 ppm, respectively) followed by a number of low-field singlets corresponding to the number of thiophene units of the bridge. Finally, products **M1**–**M3** were obtained by Stille reaction with the BDT organotin derivative. NMR and HRMS characterization was consistent with the structures of the final products. All systems but **M1** showed good thermal stability up to about 350 °C; **M1** showed 4.5% weight loss over 150 °C, with a stability plateau up to 350 °C (Figures S13–S16 in the SI).■Please check carefully. Paragraph edited to remove compound numbers■

Absorption experiments in dichloromethane (DCM) solution showed that all molecules present a broad band in the 400–500 nm region peaking ■with a maximum■ around 450 nm (Figure 1 top and Figure S11 in the SI). As the thiophene bridge increases in length, higher-energy bands decrease in intensity to finally virtually disappear or merge with the lower energy absorption band. In a way that might seem counterintuitive, this band experiences a hypsochromic shift (from $\lambda_{max} =$456 nm for **M0** to 443, 445 and 447 nm for **M1**, **M2**, and **M3**, respectively) as longer thiophene linkers are introduced between the BDT and BTD units. This behavior might be attributed to the steric hindrance induced by the dodecyl ancillary side chains linked to the thiophene spacers (vide infra), as is also observed when they are used to disrupt electronic communication in π-conjugated systems.[17] Despite this, a significant broadening of the absorption is observed for **M1**–**M3** with onsets going up to 532 nm. A completely different pattern is obtained for the absorption of thin films (Figure 1 bottom). In the case of **M0**, the λ_{max} of the thin film is red-shifted 30 nm relative to that of the DCM solution. This red-shift is ascribed to the planarization of the structure, induced by the solid-state packing of the molecules in the thin film. More important changes and the expected shift to longer wavelengths are observed in the spectra as additional thiophene units are introduced into the π-conjugated bridge. For **M1**–**M3** molecules, with increasing length of the thiophene bridge, the thin-film spectra are dominated by a broad absorption ranging from■between■ 360 to 800 nm. This band shows the characteristic vibronic structure featuring two peaks indicative of effective π–π interactions between different molecule backbones.[18]

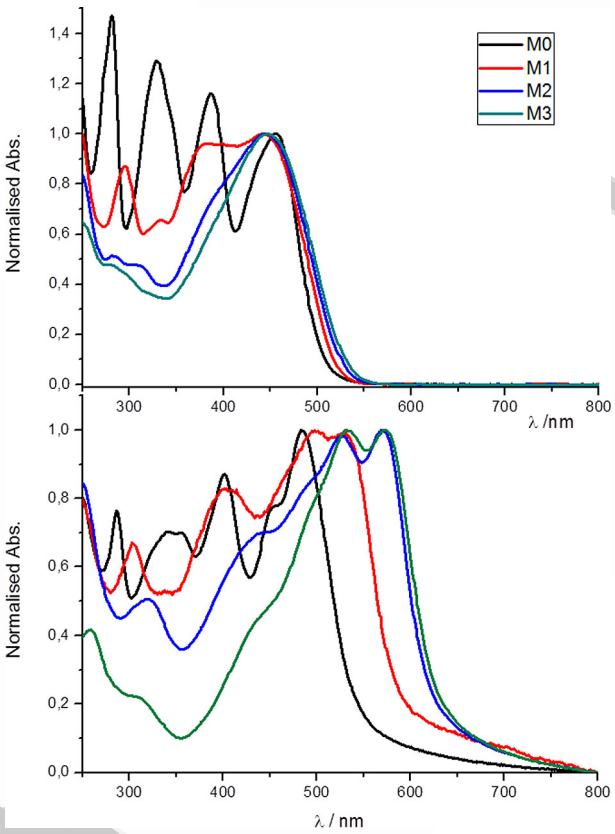

Figure 1. Normalized UV/Vis absorption spectra recorded for **M0**–**M3** in DCM solution (top) and in thin film (bottom).

The electrochemical behavior of **M0**–**M3** was studied by means of cyclic voltammetry (CV). As expected for A-D-A systems, samples showed both oxidation and reduction processes (Table 1 and Figure S12 in the SI). All molecules experience a single reversible reduction around −1.62 V with an apparently negligible effect of the thiophene bridge length. In contrast, molecules show a much more complicated behavior upon oxidation; their oxidation potentials are shifted anodically as the molecules bear more thiophene units. Compounds **M0** and **M1** show two reversible oxidation processes, whereas **M2** and **M3** show many irreversible oxidation processes (see Figure S12 in

Table 1. Redox potentials recorded for **M0**–**M3**.[a]

Compound	E^{red} [V]	$E^{ox,1}$ [V]	$E^{ox,2}$ [V]
M0	−1.614	0.835	1.204
M1	−1.614	0.735	0.957
M2	−1.633	0.659	0.815
M3	−1.611	0.615	0.769

[a] Measured by CV in CH_2Cl_2 solution using 0.1 M Bu_4NPF_6 as the supporting electrolyte, glassy carbon as the working electrode, Pt wires as counter and reference electrodes. Fc was added as internal standard recording $E_{1/2}$ = 0.284 V for the Fc/Fc^+ process.

the SI) presumably due to the mixture of states from the oligothiophene bridge and the BDT donor core. Frontier orbital energies and electrochemical gaps were estimated from the redox potential onsets (Table S3 in the SI). The energy of the highest occupied molecular orbital (HOMO)increases as more thiophene units are introduced into the bridge, ranging from −5.24 to −5.04 eV. The energies calculated for the lowest unoccupied molecular orbital (LUMO) by using either electronic or electrochemical gaps show good agreement and, as expected, are negligibly affected by the bridge size.

To shed light onto the optical and electronic properties of **M0**–**M3**, quantum chemistry calculations were performed for the isolated molecules within the density functional theory (DFT) framework. The aliphatic chains attached to the BDT core and the thiophene rings were replaced with methyl groups to alleviate the computational cost■effort■. C_i symmetry constraints were imposed for all compounds. Geometry optimizations at the B3LYP/cc-pVDZ level indicate that the minimum-energy structures of the A-D-A derivatives are mainly planar, showing small twisting angles (<20°) between adjacent rings due to short H···H (2.3 Å) and H···S (2.7–2.9 Å) contacts (Figure 2 for **M1** and Figure S18 in the SI for the rest of compounds).

Figure 3 shows the frontier molecular orbital energy diagrams calculated for **M0**–**M3**, along with representative examples of the molecular orbitals' topology for the **M1** derivative. The HOMO and HOMO−1 are localized on the electron-donor

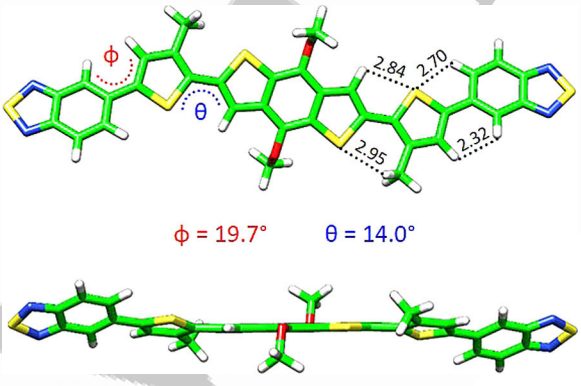

Figure 2. Top and side views of the minimum-energy geometry calculated for the **M1** derivative, including the values of dihedral angles Φ and θ and relevant inter-ring short contacts (in Å).

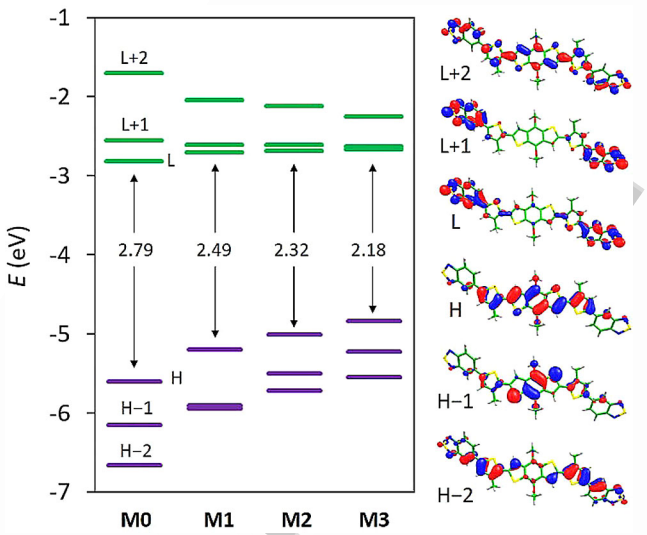

Figure 3. Frontier molecular orbital diagram including the HOMO–LUMO gap (left) and the isovalue contours (±0.03 a.u.) calculated for the **M1** derivative (right). H and L denote HOMO and LUMO, respectively.

BDT unit with some contribution from the thiophene π-conjugated bridge, whereas the HOMO−2 mainly spreads over the bridge. Conversely, the LUMO and LUMO+1 are fully located on the electron-acceptor BTD moieties, whereas the LUMO+2 spreads over the whole molecule. The description of the frontier MOs is maintained in derivatives **M0**, **M2**, and **M3**, although the nature of HOMO−1 and HOMO−2 is predicted to be swapped in **M2** and **M3** (see Figures S19 and S20 in the SI). This swap stems from the larger increase in energy the orbital located over the thiophene spacer experiences with increased spacer length, compared to the energy of the orbital localized over the BDT core (Figure 3). The HOMO energy systematically increases on going from **M0** (−5.60 eV) to **M3** (−4.84 eV) with increasing numbers of thiophene units in the π-conjugated bridge. This trend is in good accordance with the anodic shift recorded experimentally for $E^{ox,1}$ (Table 1). In contrast, the LUMO and LUMO+1 are predicted to remain practically unaltered at ca. −2.7 eV, regardless of the length of the thiophene π-spacer, due to the localization of these orbitals over the electron-acceptor BTD units. This is also in good agreement with the CV experiments. As expected, the energy difference between the LUMO and LUMO+1 decreases as the electron-acceptor moieties get more separated, reaching practically the degeneracy■and the MOs become practically degenerate■ for **M3** (Figure 3). The HOMO–LUMO gap is predicted to significantly narrow from 2.79 eV in **M0** to 2.18 eV in **M3**. The theoretical trends calculated for the HOMO–LUMO gap and the HOMO and LUMO energies along the **M0**–**M3** series are in good agreement with the experimental trends obtained from optical and electrochemical data (Table S3 in the SI).

To highlight the effect that the linking position of the BTD units has on the electronic properties, the two BTD-BDT-BTD derivatives recently reported by Du et al.,[15d] which present a structure similar to **M2** with the BTD units linked at the 4,7-positions, were also calculated at the B3LYP/cc-pVDZ level. The

main structural effect of the 4,7-substitution pattern is that the BTD units are less twisted from planarity (twisting angles of only 0.5–1.5°, Figure S21 in the SI) than in **M1**–**M3** (twisting angles in the 16–22° range, Figure 2 and Figure S18) in which the BTD units are linked in 5-position. The 4,7-substitution pattern leads to a significant reduction of the HOMO–LUMO gap (2.07 and 2.22 eV, depending on the inner or end-capping position of the BDT units, respectively; Figure S23 in the SI) compared to **M2** (2.32 eV). The narrowing of the HOMO–LUMO gap stems from a lowering of the LUMO energy due to the coplanarity of the BTD moieties in the π-conjugated path.

Time-dependent DFT (TD-DFT) calculations of the singlet excited states (S_n) were conducted to fully rationalize the nature and trends experimentally recorded for the low-lying absorption bands of **M0**–**M3**. Theoretical calculations at the TD-B3LYP/cc-pVDZ level predict for **M0** two intense electronic transitions to the low-lying excited states S_1 and S_3 at 2.50 and 2.97 eV with oscillator strengths of $f = 0.590$ and 0.485, respectively (Table 2). The $S_0 \rightarrow S_1$ and $S_0 \rightarrow S_3$ transitions are best described by one-electron promotions from the HOMO and HOMO−1 to the LUMO, respectively, which mainly imply a charge transfer (CT) from the electron-donor BDT moiety to the electron-acceptor BTD units, and give rise to the experimental bands recorded at 456 and 387 nm in DCM for **M0** (Figure 1). Moving to higher energies, the electronic transitions to S_5 and S_{10}, predicted at 3.52 and 3.95 eV, respectively, with relatively high oscillator strength ($f > 0.35$), lead to the peak experimentally recorded at 329 nm (Figure 1), and are mainly centered on the electron-donor BDT unit (Table 2 and Figure 3). A large number of high-energy electronic states calculated at energies higher than 5.0 eV explain the spectroscopic features recorded for **M0** below 300 nm (see Figure S22 in the SI).

Table 2. Lowest-lying singlet excited states calculated for **M0**–**M3** at the TD-B3LYP/cc-pVDZ level. Vertical excitation energies (*E*), oscillator strengths (*f*), description in terms of monoexcitations (contributions within parentheses), and nature of the excited state are summarized. Only the most relevant S1 and S3 states are included for **M1**–**M3**.

	State	*E* [eV]	*E* [nm]	*f*	Description	[%]	Nature
M0	S_1	2.502	496	0.5896	H→L	(96)	CT
	S_2	2.719	456	0.0000	H→L+1	(97)	CT
	S_3	2.968	418	0.4849	H−1→L	(95)	CT
	S_5	3.515	353	0.3641	H→L+2	(96)	donor
	S_{10}	3.950	314	0.3978	H−1→L+2	(87)	donor
M1	S_1	2.215	560	0.9674	H→L	(99)	CT
	S_3	2.860	434	1.0985	H→L+2	(95)	donor (CT)
M2	S_1	2.069	599	1.7438	H→L	(98)	CT
	S_3	2.600	477	1.3371	H→L+2	(80)	donor (CT)
M3	S_1	1.942	639	2.0687	H→L	(94)	CT
	S_3	2.316	535	1.7056	H→L+2	(86)	donor (CT)

Moving from **M0** to **M1**–**M3**, TD-DFT calculations predict a significant increase in the oscillator strength of the electronic transitions associated with the bright■correct?■ lowest-lying S_1 and S_3 states (Table 2 and Figure S24) due to the extension of the thiophene π-conjugated bridge. These electronic transitions, which are computed with a large CT nature■contribution, component?■, are predicted to undergo a significant red-shift to longer wavelengths (lower energies) upon extension of the thiophene bridge. The $S_0 \rightarrow S_1$ HOMO→LUMO transition goes from 2.50 eV in **M0** to 1.94 eV in **M3** in accord with the evolution of the HOMO–LUMO gap (Figure 3) and the electrochemical data (Table 1). This trend, however, does not reproduce the hypsochromic shift experimentally recorded in DCM (Figure 1 top) as longer thiophene linkers are introduced in between the BDT and BTD units. The inconsistency might in principle be attributed to the deviation of the conjugated backbone from planarity which can occur in solution due to the steric hindrance■repulsion■ induced by the dodecyl ancillary side chains attached to the thiophene spacers. Theoretical calculations were performed in order to analyze the effect that the inter-ring twisting angles between the thiophene rings and the BTD units have over the absorption features in the low-energy range (see the Experimental Section for computational details). Figure 4 displays the evolution of the energy

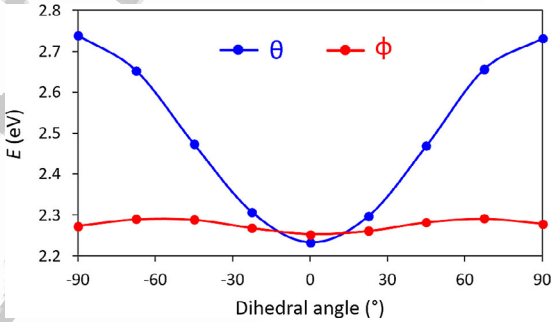

Figure 4. Evolution of the energy calculated for lowest-lying singlet excited state S_1 of the **M1** derivative as a function of the inter-ring twisting angles Φ and θ. See Figure 2 for the definition of Φ and θ.

calculated for the lowest-lying S_1 excited state as a function of the two twisting angles Φ and θ characterizing the rotational isomerism of the **M1** derivative (Figure 2). Similar studies were performed for **M0**, **M2**, and **M3** (Figure S26 in the SI). Theoretical calculations at the B3LYP/cc-pVDZ level indicate that the internal rotation of the first thiophene ring with respect to the BTD unit (Φ angle) barely impacts on the lowest-lying S_1 energy. Conversely, the variation of θ angle between the thiophene units provokes a significant shift to higher energies of the CT S_1 state, which is calculated going from 2.19 eV (530 nm) at 0° to 2.68 eV (460 nm) at 90°. Considering that the long aliphatic chains can lead to large distortions from planarity in solution, the theoretical red-shift (0.56 eV from **M0** to **M3**) predicted for S_1 upon increasing spacer length might be counterbalanced by the blue-shift resulting from the nonplanarity of the bridge (up to 0.49 eV in **M1**). This would explain the spectroscopic features observed for the lowest-lying absorption band in solution (Figure 1, top). In the thin film, effective π–π intermolecular interactions induce the planarization of the π-conjugated spacer, thus causing this band to undergo the

expected red-shift of ca. 0.4 eV moving from **M0** to **M3** (Figure 1 bottom).

To assess the electronic conductivity and the charge carrier mobility of electrons and holes, time-resolved microwave conductivity (TRMC) measurements were performed on pristine solid films of compounds **M0**–**M3** under 355 nm excitation (Figure 5). The photoconductivity maxima depend on the

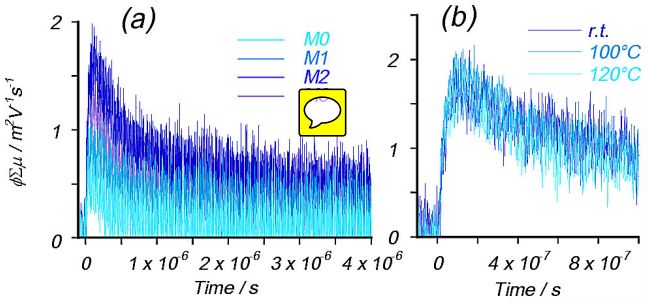

Figure 5. a) Kinetic traces of transient conductivity ($\varphi\Sigma\mu$; product of photocarrier generation yield (φ) and the sum of mobilities ($\Sigma\mu$)) observed for the series of compounds **M0**–**M3** under 355 nm excitation after annealing at 120 °C. b) Kinetic traces observed for compound **M2** before and after thermal annealing.■graphic ok?■

length of the thiophene bridge, maximizing for **M2**. Noteworthy, observed kinetic traces for all compounds of the series seem to almost overlap, meaning an almost negligible effect of the thiophene bridge length, without significant acceleration in the case of the shortest bridged compound (**M0**). Altogether, this suggests that the kinetics are due to bulk recombination of the photo-generated free charge carriers. Optimization of photoconductivity was also examined by thermal annealing of the best performing material (**M2**), which showed no significant change in its conductivity before/after the annealing. This is also confirmed by the identical XRD patterns observed during the annealing processes. XRD analyses demonstrate that the above-mentioned solid-state π–π interactions induce highly ordered crystalline films featuring the characteristic (100) low-angle diffractions (see Figure■ok?■ S17 in the SI).

Reorganization energies (λ) were calculated at the B3LYP/cc-pVDZ level to give insight into the hole and electron transport ability of the A-D-A derivatives **M0**–**M3** (Table 3, see the Experimental Section and Figure S27 in the SI for computational details). Theoretical calculations indicate that hole reorganization energies (λ_{hole}) for our derivatives are above 0.2 eV, suggesting a limited ability for hole transport. In contrast, electron reorganization energies ($\lambda_{electron}$) are predicted in the range of 0.11–0.17 eV. These $\lambda_{electron}$ values are as small as that obtained for fullerene C_{60} (0.129 eV) at the same level of theory (reported value of 0.13 eV),[19] pointing to BDT-BTD **M0**–**M3** derivatives as efficient electron-transporting materials. When the π-conjugated spacer is extended, both λ_{hole} and $\lambda_{electron}$ diminish, suggesting that transport properties improve from **M1** to **M3**. It should be mentioned that the thiophene bridges are involved in forming both the cation and the anion species. For instance, 0.63 e is extracted from the terthiophene bridges for **M3** upon oxidation to **M3**$^+$ and 0.44 e is introduced upon reduction to **M3**$^-$. Notwithstanding■Regardless, Nevertheless■, charge carrier mobilities will ultimately be determined by the supramolecular arrangement of the derivatives in the films.

Table 3. Reorganization energies (λ, in eV) related to the transport of holes (λ_{hole}) and electrons ($\lambda_{electron}$) calculated at the B3LYP/cc-pVDZ level of theory.

	M0	M1	M2	M3
λ_{hole}	0.235	0.278	0.252	0.216
$\lambda_{electron}$	0.162	0.173	0.138	0.115

Based on the good film-forming properties of compound **M2** and the interesting results obtained from the theoretical calculations, we examined the quantitative contributions from positive and negative charge carriers to the semiconducting nature of the compound by time-resolved microwave conductivity (TRMC) measurements at interfaces with the simple metal–insulator semiconductor device. In this system, positive and negative charge carriers are separately injected through ultrathin electrodes by the applied modulated bias, and are accumulated at the semiconductor–insulator interface. The local motion of the selectively injected charge carriers was traced by noncontact 9 GHz microwave probes, directly providing the product of number (n) and mobility (μ) of the injected charge carriers. Figure S28 in the SI shows the observed microwave absorption in the case of hole and electron injection, separately. It is noteworthy that the device is completely silent for hole injection as much as ca. 0.05 nC, but active for electron injection in agreement with the theoretically predicted low $\lambda_{electron}$ values (significantly smaller than λ_{hole}, Table 3). This is suggestive of the n-type semiconducting nature of the compound with its mobility μ in the range of ca. 0.1 cm^2V^{-1s-1}.

In summary, we have presented BDT–BTD oligomers with a low band gap of about 2.0 eV, broad absorption in the 400–750 nm region, and good thermal stability. These materials form highly ordered crystalline films, evidenced by the vibronic structure of the UV/Vis absorption spectra and confirmed by XRD measurements. Interestingly, these BDT–BTD small molecules featuring A-D-A architectures behave as n-channel charge transporters, showing high electron mobilities $\mu_e \approx 0.1$ $cm^2V^{-1}s^{-1}$. Considering that organic semiconducting materials often exhibit electron mobilities one to two orders of magnitude lower, these molecules may well be suitable candidates for photoelectric conversion.

Experimental Section

Materials and methods

Materials obtained from commercial suppliers were used without further purification. Solvents were dried and degassed following standard procedures. Air-sensitive reactions were carried out under argon atmosphere. Flash chromatography was performed using silica gel (Fluorochem, Silicagel 60A, 40–63 micron). Analytical thin-layer chromatography (TLC) was performed using aluminum-coated Merck Kieselgel 60 F254 plates. NMR spectra were recorded

on a Bruker Advance 300 (^{1}H: 400 MHz; ^{13}C: 101 MHz) spectrometer at 298 K using partially deuterated solvents as internal standards. Multiplicities are denoted as follows: s = singlet, d = doublet, t = triplet, m = multiplet. FTIR spectra were recorded on a Bruker Tensor 27 (ATR device) spectrometer. UV/Vis spectra were recorded in a Varian Cary 50 spectrophotometer. Mass spectra and matrix-assisted laser desorption ionization (coupled to a time-of-flight analyzer) (MALDI-TOF) mass spectra were recorded on a MAT 95 thermo-spectrometer and a Bruker REFLEX spectrometer, respectively■ok?■. Cyclic voltammetry (CV) experiments were conducted in a 0.1 M solution of NBu_4PF_6 in DCM. A glassy carbon electrode was used as the working electrode and platinum wires were used as counter and reference electrodes. Before each measurement, solutions were deoxygenated with N_2. Ferrocene was added as an internal standard.

Theoretical calculations

Calculations were performed for the BDT–BTD A-D-A derivatives under the density functional theory (DFT) framework using the Gaussian 09 (version D01) suite of programs.[20] The well-established hybrid exchange-correlation B3LYP functional[21] was used in combination with the correlation-consistent Dunning's cc-pVDZ basis set.[22] First, fully relaxed minimum-energy structures were obtained at the B3LYP/cc-pVDZ level in the gas phase and making use■taking advantage■ of the C_i symmetry point group. Molecular orbitals were depicted by means of the Chemcraft 1.6 software[23] using isovalue contours of ±0.03 a.u.

Time-dependent DFT (TDDFT) calculations[24] were carried out for the A-D-A systems at the B3LYP/cc-pVDZ level in the gas phase. The 60 lowest-lying singlet excited states were computed. The TDDFT simulations presented in Figures S22 and S23 in the SI were generated by convoluting each electronic transition with a Gaussian function of full-width-at-half-maximum (FWHM) of 0.20 eV. A rigid scan of the inter-ring twisting angles characterizing the rotational isomerism of the π-conjugated A-D-A backbone was performed at the B3LYP/cc-pVDZ level to analyze their influence on the lowest-lying singlet excited state (S_1). Due to the C_i symmetry used for the **M0**–**M3** derivatives, identical values from −90° to 0° to +90° were set for equivalent twisting angles on both halves of the molecule (Figure 4 and Figure S24). For the definition of the inter-ring twisting angles, see Figure 2 and Figure S19.

Theoretical reorganization energies for the hole (λ_{hole}) and electron ($\lambda_{electron}$) transport of **M0**–**M3** derivatives were calculated at the B3LYP/cc-pVDZ level according to the scheme depicted in Figure S18. The intramolecular reorganization energy (λ) consists of two terms related to the geometry relaxation energies of a molecule on going from the fully relaxed ground state of the neutral species to the charged state (cation or anion), and a neighboring molecule evolving in the opposite way.[25] Thus, λ_{hole} and $\lambda_{electron}$ in a molecular system can be defined by Equations (1) and (2), respectively,

$$\lambda_{hole} = \lambda_1^+ + \lambda_2^+ = \left(E_N^{+1} - E_C^{+1}\right) + \left(E_C^0 - E_N^0\right) \quad (1)$$

$$\lambda_{electron} = \lambda_1^- + \lambda_2^- = \left(E_N^{-1} - E_C^{-1}\right) + \left(E_C^0 - E_N^0\right) \quad (2)$$

where E_Y^X is the energy of the neutral ($X=0$), cation ($X=+1$), or anion ($X=-1$) species at the minimum-energy geometry of the neutral ($Y=N$) or the corresponding charged species ($Y=C$), and λ_1 and λ_2 are the two contributions to the total intramolecular reorganization energy (λ). The cation and anion species were computed as doublet open-shell species using the spin-unrestricted UB3LYP approach.

Fabrication of films for flash-photolysis time-resolved microwave conductivity (FP-TRMC) measurements

All the compounds were dissolved in toluene and spin-coated onto quartz substrates (9×40 mm², 1 mm thick). The films were dried under vacuum ($<2\times10^{-1}$ Pa) for 1 h to remove residual solvent, and successively annealed at 100 °C.

Measurement of FP-TRMC at interfaces[3,26]

Charge carrier mobility was evaluated by FP-TRMC at room temperature under Ar-saturated conditions. Charge carriers were photochemically generated using a third harmonic generation (λ = 355 nm) of a Spectra Physics model INDI-HG Nd:YAG laser with a pulse duration of 5–8 ns and frequency of 10 Hz. The photon density of a 355 nm pulse was 9.1×10^{15} photons cm^{-2} pulse^{-1}. The microwave frequency and power were set at ca. 9.1 GHz and 3 mW, respectively, and guided into a microwave cavity with Q-factor of 2200, where the substrate with the compound films were set at the point of electric field maximum. The reflected power of the probing microwave, picked up by a diode (rise time <1 ns), was monitored by a Tektronics model TDS3032B digital oscilloscope after amplification by Ciao Electronics CA812-304 FET amplifier system. The observed change in the reflected microwave power (ΔP_r) was normalized with the steady reflection of the microwave from the cavity (P_r), and converted into $\varphi\Sigma\mu = (1/eAI_0F_{light})(\Delta P_r/P_r)$, where e, A, I_0, F_{light}, φ, and $\Sigma\mu$ are elementary charge, sensitivity factor (S^{-1} cm), incident photon density of the excitation laser (photon cm^{-2}), filling factor (cm^{-1}), a photocarrier generation yield, and the sum of the charge carrier mobilities. The value of F_{light} was calculated based on the overlap of active area of the sample with electric field strength distribution in the cavity derived from a calculation code of CST Microwave Studio from AET Inc.

Fabrication of metal–insulator semiconductor (MIS) devices

The MIS devices of the compounds were fabricated as follows: 1) a quartz substrate (4.9×50 mm², 1 mm thick) was cleaned with UV-O_3; 2) Ti and Au (gate electrode, 5 and 30 nm, respectively) layers were successively deposited on the quartz substrate by DC sputtering and thermal vacuum deposition, respectively; 3) as an insulating layer, a 350-nm-thick polyimide (U-imide, UNITIKA Co. Ltd.) was doubly overcoated as■to■ the total thickness of 700 nm; 4) the compound **M2** was spin-coated from the corresponding toluene solutions to reach a thickness of 30–50 nm, and dried under vacuum $<2\times10^{-4}$ Pa for 1 h; and 5) a 30-nm-thick top Au electrode was overcoated■applied■ by vacuum deposition.

Measurement of TRMC at interfaces

The microwave circuit was constructed using a waveguide system with homodyne setup and the signal was picked up by a Schottky diode.[27] The TRMC at interfaces measurements were carried out with a microwave at 9 GHz from a signal generator (Rohde & Schwarz, SMF 100A). After the MIS device was loaded in the microwave cavity, a pulse gate bias voltage $V_g(t)$ at an interval of 50 ms was applied based on a multifunction generator (NF Corporation, WF 1973). The response of the reflected microwave power ($\Delta P_r(t)$)

due to accumulated charge carriers at the interface and the current injected into the semiconductor–insulator interface ($I(t)$) were monitored using a digital phosphor oscilloscope (Tektronix, MDO 3022). All experiments were conducted under ambient atmosphere at room temperature.

XRD measurements

XRD patterns of the films on quartz substrates were measured by a Rigaku model MiniFlex600 X-ray diffractometer equipped with a X-ray tube using a Cu Kα radiation beam with a wavelength of 1.54 Å and a semiconductor detector (Rigaku, D/teX Ultra). Diffraction intensities were recorded with 0.02° steps in 2θ.

Acknowledgements

This study was funded by the European Commission (ERC-320441-Chirallcarbon), the MINECO of Spain (CTQ2014-52045-R, CTQ2015-71154-P, and Unidad de Excelencia María de Maeztu MDM-2015-0538), the Comunidad de Madrid (FOTOCARBON-CM S2013/MIT-2841), the Generalitat Valenciana (PROMETEO/2016/135), and European FEDER funds (CTQ2015-71154-P). J.C. thanks the MECD of Spain for a predoctoral FPU grant. N.M. thanks EC FP7 ITN "MOLESCO" Project No. 606728.

Conflict of interest

The authors declare no conflict of interest.

Keywords: donor–acceptor systems · conducting materials · density functional calculations · donor–acceptor systems · electrochemistry

[1] a) Y. Olivier, D. Niedzialek, V. Lemaur, W. Pisula, K. Müllen, U. Koldemir, J. R. Reynolds, R. Lazzaroni, J. Cornil, D. Beljonne, *Adv. Mater.* **2014**, *26*, 2119 – 2136; b) H. Sirringhaus, *Adv. Mater.* **2014**, *26*, 1319 – 1335; c) Y. Tsutsui, G. Schweicher, B. Chattopadhyay, T. Sakurai, J.-B. Arlin, C. Ruzié, A. Aliev, A. Ciesielski, S. Colella, A. R. Kennedy, V. Lemaur, Y. Olivier, R. Hadji, L. Sanguinet, F. Castet, D. Beljonne, J. Cornil, P. Samorì, S. Seki, Y. H. Geerts, *Adv. Mater.* **2016**, *28*, 7106 – 7114.

[2] a) S. Li, L. Ye, W. Zhao, S. Zhang, S. Mukherjee, H. Ade, J. Hou, *Adv. Mater.* **2016**, *28*, 9423 – 9429; b) J. Huang, J. H. Carpenter, C.-Z. Li, J.-S. Yu, H. Ade, A. K.-Y. Jen, *Adv. Mater.* **2016**, *28*, 967 – 974; c) B. Fan, W. Zhong, X.-F. Jiang, Q. Yin, L. Ying, F. Huang, Y. Cao, *Adv. Energy Mater.* **2017**, DOI: 10.1002/aenm.201602127■■update?■■.

[3] a) Y. Kiyota, T. Kadoya, K. Yamamoto, K. Iijima, T. Higashino, T. Kawamoto, K. Takimiya, T. Mori, *J. Am. Chem. Soc.* **2016**, *138*, 3920 – 3925; b) D. Huang, C. Wang, Y. Zou, X. Shen, Y. Zang, H. Shen, X. Gao, Y. Yi, W. Xu, C. Di, D. Zhu, *Angew. Chem. Int. Ed.* **2016**, *55*, 10672 – 10675; *Angew. Chem.* **2016**, *128*, 10830 – 10833.

[4] a) B. C. Thompson, Y. G. Kim, T. D. McCarley, J. R. Reynolds, *J. Am. Chem. Soc.* **2006**, *128*, 12714 – 12725; b) G. Lu, H. Usta, C. Risko, L. Wang, A. Facchetti, M. A. Ratner, T. J. Marks, *J. Am. Chem. Soc.* **2008**, *130*, 7670 – 7685; c) H. Y. Chen, J. H. Hou, S. Q. Zhang, Y. Y. Liang, G. W. Yang, Y. Yang, L. P. Yu, Y. Wu, G. Li, *Nat. Photonics* **2009**, *3*, 649 – 653; d) I. McCulloch, M. Heeney, M. L. Chabinyc, D. DeLongchamp, R. J. Kline, M. Coelle, W. Duffy, D. Fischer, D. Gundlach, B. Hamadani, R. Hamilton, L. Richter, A. Salleo, M. Shkunov, D. Sporrowe, S. Tierney, W. Zhong, *Adv. Mater.* **2009**, *21*, 1091 – 1109; e) S. C. Price, A. C. Stuart, W. You, *Macromolecules* **2010**, *43*, 4609 – 4612.

[5] S. Mataka, K. Takahashi, T. Imura, M. Tashiro, *J. Heterocycl. Chem.* **1982**, *19*, 1481 – 1488.

[6] T. Balasankar, M. Gopalakrishnan, S. Nagarajan, *Eur. J. Med. Chem.* **2005**, *40*, 728 – 731.

[7] A. Rocher, C. Dumas, J. M. Cock, *Gene* **2005**, *344*, 181 – 192.

[8] T. S. van der Poll, J. A. Love, T.-Q. Nguyen, G. C. Bazan, *Adv. Mater.* **2012**, *24*, 3646 – 3649.

[9] J.-L. Wang, Q.-R. Yin, J.-S. Miao, Z. Wu, Z.-F. Chang, Y. Cao, R.-B. Zhang, J.-Y. Wang, H.-B. Wu, Y. Cao, *Adv. Funct. Mater.* **2015**, *25*, 3514 – 3523.

[10] H. Hu, K. Jiang, G. Yang, J. Liu, Z. Li, H. Lin, Y. Liu, J. Zhao, J. Zhang, F. Huang, Y. Qu, W. Ma, H. Yan, *J. Am. Chem. Soc.* **2015**, *137*, 14149 – 14157.

[11] Y. Liu, J. Zhao, Z. Li, C. Mu, W. Ma, H. Hu, K. Jiang, H. Lin, H. Ade, H. Yan, *Nat. Commun.* **2014**, *5*, 5293.

[12] P. Sonar, S. P. Singh, Y. Li, M. S. Soh, A. Dodabalapur, *Adv. Mater.* **2010**, *22*, 5409 – 5413.

[13] L. E. Polander, L. Pandey, S. Barlow, S. P. Tiwari, C. Risko, B. Kippelen, J.-L. Brédas, S. R. Marder, *J. Phys. Chem. C* **2011**, *115*, 23149 – 23163.

[14] P. M. Beaujuge, H. N. Tsao, M. R. Hansen, C. M. Amb, C. Risko, J. Subbiah, K. R. Choudhury, A. Mavrinskiy, W. Pisula, J.-L. Brédas, F. So, K. Müllen, J. R. Reynolds, *J. Am. Chem. Soc.* **2012**, *134*, 8944 – 8957.

[15] a) L. Liang, J.-T. Wang, X. Xiang, J. Ling, F.-G. Zhao, W.-S. Li, *J. Mater. Chem. A* **2014**, *2*, 15396 – 15405; b) K. Do, N. Cho, S. A. Siddiqui, S. P. Singh, G. D. Sharma, J. Ko, *Dyes Pigm.* **2015**, *120*, 126 – 135; c) L. Yuan, Y. Zhao, J. Zhang, Y. Zhang, L. Zhu, K. Lu, W. Yan, Z. Wei, *Adv. Mater.* **2015**, *27*, 4229 – 4233; d) J. Du, A. Fortney, K. E. Washington, C. Bulumulla, P. Huang, D. Dissanayake, M. C. Biewer, T. Kowalewski, M. C. Stefan, *ACS Appl. Mater. Interfaces* **2016**, *8*, 33025 – 33033.

[16] F. S. Mancilha, B. A. DaSilveira Neto, A. S. Lopes, P. F. Moreira, Jr., F. H. Quina, R. S. Gonçalves, J. Dupont, *Eur. J. Org. Chem.* **2006**, 4924 – 4933.

[17] H. Li, A. S. Batsanov, K. C. Moss, H. L. Vaughan, F. B. Dias, K. T. Kamtekar, M. R. Bryce, A. P. Monkman, *Chem. Commun.* **2010**, *46*, 4812 – 4814.

[18] J. Zhou, Y. Zuo, X. Wan, G. Long, Q. Zhang, W. Ni, Y. Liu, Z. Li, G. He, C. Li, B. Kan, M. Li, Y. Chen, *J. Am. Chem. Soc.* **2013**, *135*, 8484 – 8487.

[19] J. J. Kwiatkowski, J. M. Frost, J. Nelson, *Nano Lett.* **2009**, *9*, 1085 – 1090.

[20] M. J. Frisch, G. W. Trucks, H. B. Schlegel, G. E. Scuseria, M. A. Robb, J. R. Cheeseman, G. Scalmani, V. Barone, B. Mennucci, G. A. Petersson, H. Nakatsuji, M. Caricato, X. Li, H. P. Hratchian, A. F. Izmaylov, J. Bloino, G. Zheng, J. L. Sonnenberg, M. Hada, M. Ehara, K. Toyota, R. Fukuda, J. Hasegawa, M. Ishida, T. Nakajima, Y. Honda, O. Kitao, H. Nakai, T. Vreven, J. A. Montgomery, J. E. Peralta, F. Ogliaro, M. Bearpark, J. J. Heyd, E. Brothers, K. N. Kudin, V. N. Staroverov, R. Kobayashi, J. Normand, K. Raghavachari, A. Rendell, J. C. Burant, S. S. Iyengar, J. Tomasi, M. Cossi, N. Rega, J. M. Millam, M. Klene, J. E. Knox, J. B. Cross, V. Bakken, C. Adamo, J. Jaramillo, R. Gomperts, R. E. Stratmann, O. Yazyev, A. J. Austin, R. Cammi, C. Pomelli, J. W. Ochterski, R. L. Martin, K. Morokuma, V. G. Zakrzewski, G. A. Voth, P. Salvador, J. J. Dannenberg, S. Dapprich, A. D. Daniels, Farkas, J. B. Foresman, J. V. Ortiz, J. Cioslowski, D. J. Fox, *Gaussian 09, Revision D.01*, Wallingford CT, **2009**.

[21] A. D. Becke, *J. Chem. Phys.* **1993**, *98*, 5648 – 5652.

[22] J. T. H. Dunning, *J. Chem. Phys.* **1989**, *90*, 1007 – 1023.

[23] G. A. Zhurko, ChemCraft 1.8, **2015**, http://www.chemcraftprog.com.

[24] a) C. Jamorski, M. E. Casida, D. R. Salahub, *J. Chem. Phys.* **1996**, *104*, 5134 – 5147; b) M. E. Casida, C. Jamorski, K. C. Casida, D. R. Salahub, *J. Chem. Phys.* **1998**, *108*, 4439 – 4449; c) M. Petersilka, U. J. Gossmann, E. K. U. Gross, *Phys. Rev. Lett.* **1996**, *76*, 1212 – 1215.

[25] J.-L. Brédas, D. Beljonne, V. Coropceanu, J. Cornil, *Chem. Rev.* **2004**, *104*, 4971 – 5004.

[26] S. Seki, A. Saeki, T. Sakurai, D. Sakamaki, *Phys. Chem. Chem. Phys.* **2014**, *16*, 11093 – 11113.

[27] a) Y. Honsho, T. Miyakai, T. Sakurai, A. Saeki, S. Seki, *Sci. Rep.* **2013**, *3*, 3182; b) W. Choi, T. Miyakai, T. Sakurai, A. Saeki, M. Yokoyama, S. Seki, *Appl. Phys. Lett.* **2014**, *105*, 033302; c) J. Inoue, Y. Tsutsui, W. Choi, K. Kubota, T. Sakurai, S. Seki, *ACS Omega*, ~~in press■■update with DOI needed■■~~.

Manuscript received: January 31, 2017
Revised: February 22, 2017
Accepted Article published: ■■ ■■, 0000
Final Article published: ■■ ■■, 0000

R. Sandoval-Torrientes, J. Calbo, W. Matsuda, W. Choi, J. Santos, S. Seki, E. Ortí,* N. Martín**

■■ – ■■

Efficient Benzodithiophene/ Benzothiadiazole-Based n-Channel Charge Transporters

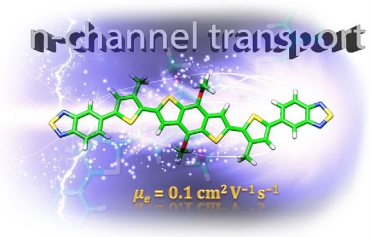

Getting electrons on the move: Acceptor-donor-acceptor triads based on benzothiadiazole and benzodithiophene moieties show unprecedented high electron mobilities (0.1 $cm^2V^{-1}s^{-1}$) for these sort of low band-gap (2.0 eV) materials. These experimental findings are explained by the calculated low reorganization energies and the good quality of the film.

Donor-acceptor-donor molecules in #thinfilms with high electron mobility Nazario Martin @IMDEA_Nano
SPACE RESERVED FOR IMAGE AND LINK

Share your work on social media! *ChemPlusChem* has added Twitter as a means to promote your article. Twitter is an online microblogging service that enables its users to send and read text-based messages of up to 140 characters, known as "tweets". Please check the pre-written tweet in the galley proofs for accuracy. Should you or your institute have a Twitter account, please let us know the appropriate username (i.e., @accountname), and we will do our best to include this information in the tweet. This tweet will be posted to the journal's Twitter account @ChemPlusChem (follow us!) upon online publication of your article, and we recommended you to repost ("retweet") it to alert other researchers about your publication.

Please check that the ORCID identifiers listed below are correct. We encourage all authors to provide an ORCID identifier for each coauthor. ORCID is a registry that provides researchers with a unique digital identifier. Some funding agencies recommend or even require the inclusion of ORCID IDs in all published articles, and authors should consult their funding agency guidelines for details. Registration is easy and free; for further information, see http://orcid.org/.

Rafael Sandoval-Torrientes
Joaquín Calbo
Wakana Matsuda
Wookjin Choi
Dr. José Santos http://orcid.org/0000-0002-9702-2315
Prof. Dr. Shu Seki
Prof. Enrique Ortí
Prof. Nazario Martín http://orcid.org/0000-0002-5355-1477

Author Contributions

J.S. Writing – original draft: Lead; Writing – review & editing: Lead
E.O. Writing – review & editing: Supporting
N.M. Writing – review & editing: Supporting.